HIV-1 genome trafficking initiates APOBEC3G packaging in the cytosol

Jordan T. Becker, Edward L. Evans III, Bayleigh E. Benner, Stephanie L. Fricke, Laura E. Smith, Andra E. Bates, & Nathan M. Sherer*

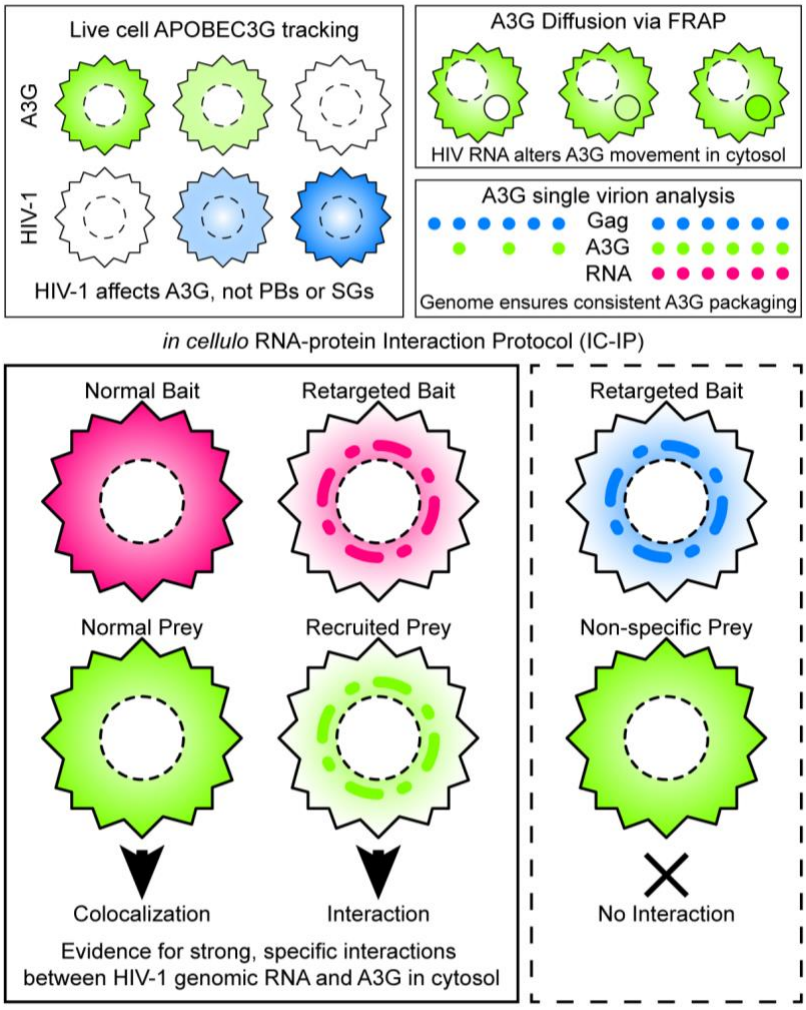

McArdle Laboratory for Cancer Research, Institute for Molecular Virology, and Carbone Cancer Center
University of Wisconsin – Madison
1525 Linden Drive, Madison, WI 53706

Short title: HIV-1 RNA genome regulates A3G trafficking

*To whom correspondence should be addressed: 501 Robert M. Bock Lab, 1525 Linden Drive, Madison, WI 53706. Tel: (608) 890-2551. Email: nsherer@wisc.edu

ABSTRACT

HIV-1 RNA genomes interact with diverse RNA binding proteins in the cytoplasm including antiviral factor APOBEC3G (A3G) that, in the absence of viral Vif proteins, is packaged into virions. When and where genome-A3G interactions are initiated in the host cell is unknown. Here we use quantitative long-term (>24 h) live cell fluorescence video microscopy and a new in-cell RNA-protein interaction assay (the “IC-IP”) to describe subcellular viral and A3G trafficking behaviors over the entire HIV-1 productive phase. Among other findings, we demonstrate that genome-A3G interactions are initiated in the cytosol soon if not immediately after genome nuclear export; that A3G-genome interactions are sufficiently strong so that tethering either factor to membranes inhibits trafficking of the reciprocal binding partner; and that selective recognition of genomes promotes consistent delivery of A3G to sites of virion assembly. Further elucidation of RNA signature(s) detected by A3G may inform development of RNA-targeted antivirals.

INTRODUCTION

The human immunodeficiency virus type 1 (HIV-1) hijacks a diverse set of host cellular RNA binding proteins (RBPs) to carry out viral RNA transcription, nuclear export, translation, and trafficking[1–4]. Select host RBPs are packaged into virions and exhibit antiviral properties, with the best-characterized example being members of the Apolipoprotein B mRNA editing enzyme, catalytic polypeptide-like 3 (APOBEC3) family. A subset of APOBEC3 proteins (A3F, A3G, and A3H) are packaged into virions to abolish infectivity by deaminating cytidines on the nascent minus-sense DNA strand of the viral genome, thereby generating G-to-A mutations in the DNA provirus[5–8]. During productive infection, however, APOBEC3 proteins are counteracted by viral infectivity factor (Vif) proteins that facilitate their proteasome-mediated degradation prior to the onset of virus particle production[9–11].

How A3G proteins is delivered to virions in the absence of Vif remains a poorly understood aspect of the cell-intrinsic host defense. HIV-1 virion assembly is driven by viral Gag capsid proteins multimerizing on an RNA scaffold consisting of host-derived RNA molecules and two dimerized viral RNA genomes, with Gag-RNA binding mediated by Gag's C-terminal Nucleocapsid (NC) domain [reviewed in [12]]. In the absence of viral genomes, Gag expression is sufficient to drive formation of non-infectious particles containing cellular RNAs, packaged in proportion to their relative abundance in the cell[13,14]. A3G's incorporation into virions has been shown, for most cell types, to be both RNA- and NC-dependent[15–20]. However, the relative contributions of genomes vs. host RNAs to this process remains controversial. On the one hand, A3G-RNA binding is relatively promiscuous, with A3G incorporated into virus particles even when packageable

genomes are not expressed[17,19]. On the other hand, A3G incorporation levels are moderately enhanced when genomes are present[16,21]; and A3G has been shown to exhibit selective RNA-binding characteristics[19,22] including a reported preference for G-rich segments of the HIV-1 genome[20].

Where and when A3G interfaces with Gag and/or genomes in the cell has also been under investigation for some time with conflicting results. At steady-state, A3G is distributed throughout the cytosol (the aqueous phase of the cytoplasm) and accumulates to high levels at non-membranous cytoplasmic sites of mRNA decay known as processing bodies (PBs)[23,24]. Cytosolic A3G is also rapidly re-localized to sites of translational repression known as stress granules (SGs) in response to heat shock or oxidative stress[23,24]. Initial studies proposed a functional link between PBs and A3G's antiviral activity[23,25,26]. By contrast, more recent work has shown visible PBs to have little to no discernible relevance to the HIV-1 life cycle[27,28].

The dynamic and complex nature of cytoplasmic RNA trafficking during HIV-1 virion genesis may have obscured consistent prior observations made in fixed cells, emphasizing a need for real-time characterization the host RBP response to HIV-1 infection at subcellular resolution. Accordingly, herein we set out to comprehensively define the behaviors of HIV-1 RNA genomes, Gag, A3G, and additional PB and SG markers over the entire viral productive phase using long-term (>24h) live cell video microscopy. Our results expose single-cell A3G degradation and trafficking behaviors in the presence or absence of Vif; and show that HIV-1 infection has little to no net effect on cytoplasmic PBs or SG formation. Fluorescence recovery after photobleaching (FRAP) and a new in-cell RNA-protein interaction assay indicate that A3G-genome interactions

76 are strong, specific, Gag-independent, and initiated in a non-localized fashion throughout
77 the cytosol long before the onset of virus particle assembly. Importantly, A3G-genome
78 interactions were sufficiently strong so that artificially tethering A3G to membranes
79 sequestered genomes in the cytoplasm and inhibited HIV-1 virus particle production.
80 Finally, using single virion analysis, we demonstrate that while genomes are not essential
81 for A3G packaging, their presence promotes a more consistent per virion delivery of A3G
82 to sites of virus particle assembly. We discuss the potential implications of A3G's selective
83 recognition of RNA in the host cytosol, and how these principles might be exploited to
84 suppress genome trafficking and virus replication *in vivo*.
85

RESULTS

Tracking HIV-1 replication using a YFP-A3G biosensor cell line. To study real-time RBP responses to HIV-1 in single cells over an entire round of viral replication, we generated "biosensor" HeLa cell lines stably expressing fluorescent protein-tagged versions of A3G (YFP-A3G) (Fig 1a) or relevant cytoplasmic RBPs including TIA1-YFP (a marker of SGs) (Fig. 2a) and CFP-DCP1A (a marker of PBs) (Fig. 2e)[24,29]. Cells were infected with either of two versions of an HIV-1_{NL4-3} reporter virus modified to express cyan fluorescent protein (CFP) from the *nef* locus (as a marker of early viral gene expression); either; (1) Vif-competent (Vif+) virus; or (2) a virus rendered Vif-minus (Vifxx) due to insertion of two stop codons in the *vif* reading frame (see cartoon depiction in Fig 1b). In the absence of virus, YFP-A3G was localized to the cytoplasm and accumulated in bright foci consistent with PBs, as anticipated (Fig. 1a, left panel). Induction of oxidative stress using 250 μM sodium arsenite (Ars)[30] caused YFP-A3G to accumulate in SGs, confirming an intact stress response (Fig. 1a, right panel). We also confirmed that our YFP-A3G fusion protein was packaged into Vifxx virus particles and retained antiviral activity using single-round assembly and infectivity assays (Fig. 1c).

In our first set of live cell imaging experiments, we infected Hela.YFP-A3G cells with Vif+ virus at a MOI of <1 in order to visualize both infected and uninfected cells side-by-side in the same field. Viral gene expression (based on detection of CFP) was initiated 12-16 hours post-infection (hpi), followed by a gradual loss of YFP-A3G signal consistent with Vif-dependent YFP-A3G proteasomal degradation (decay rate of 24.5% / h +/-6.0%; n=33; Fig. 1d, Video 1, and quantification in Fig. 1e). We observed YFP-A3G to be depleted from both the diffuse cytosolic and PB pools simultaneously, with levels

stabilized at near-background with little to no recovery, even at the latest time points (Fig.1d shows a 48h time point, with Fig.1e showing kinetics over the entire 48h time course). We also observed cell rounding at the latest time points (Fig. 1d and Video 1, see 48 h time point) consistent with real-time visualization of Vif-induced cell cycle arrest[31]. Taken together, these movies validated our use of YFP-A3G as a proxy sensor for detecting HIV-1 infection and tracking multivariate single-cell responses to Vif. Further, they exposed Vif-A3G kinetic details including: (1) that Vif's capacity to degrade A3G is potent in every single infected cell; (2) that Vif operates ubiquitously throughout the cytoplasm; and (3) that Vif's effects are remarkably persistent on a per cell basis, *i.e.*, the YFP-A3G biosensor demonstrated no discernible fluctuations to single-cell Vif activity post-YFP-A3G degradation, even over time frames of greater than 24 h.

HIV-1 infection in the absence of Vif re-localizes YFP-A3G to virion assembly sites at the plasma membrane. We next visualized YFP-A3G responses after HeLa.YFP-A3G infection with Vif-deleted (Vifxx) virus. As expected, YFP-A3G expression was maintained in the cytoplasm and at PBs throughout the entire course of infection, and cell cycle arrest was not observed (Fig. 1f and Video 2). Strikingly, however, in infected cells we observed YFP-A3G coalescing in large (up to 4 μm diameter) clusters at 30-48 hpi (Fig. 1f, white arrows highlight growing clusters). These clusters were unlikely to be PBs or SGs based on their proximity to the cell surface and real-time observations of cluster release and transfer to neighboring cells (Fig. 1f, 32h time point, and tracked in Video 2). Instead, we hypothesized that clusters represented recruitment of YFP-A3G from the cytoplasm to sites of virus particle assembly at the plasma membrane. Consistent with this hypothesis,

YFP-A3G clusters stained positive for both HIV-1 Gag/Gag-Pol and viral genome but not *YFP-A3G* mRNA (as a negative control) detected using a 4-color combined anti-p24$_{Gag}$ immunofluorescence (IF) and RNA fluorescence in situ hybridization (FISH) protocol (Fig. 1g). Thin section electron microscopy also confirmed clustering of virus particles at the surface of HeLa.YFP-A3G cells at 48 hpi for both the Vif+ and Vifxx conditions (Fig. 1h). Based on these results, we concluded that even in the absence of Vif, YFP-A3G serves as a useful proxy biosensor for detecting HIV-1 virus particle assembly through monitoring YFP-A3G's virus-driven translocation from the cytoplasm to the plasma membrane.

HIV-1 replication has little to no effect on PB integrity or SG formation. Because HIV-1 drastically alters YFP-A3G subcellular trafficking behaviors in both the presence and absence of Vif expression, we thought it important to ascertain if HIV-1 impacted the net integrity of A3G's major cytoplasmic sites of accumulation, *i.e.*, SGs and PBs. To address this question, we monitored Vif+ and Vifxx HIV-1 infection of two biosensor cell lines engineered to stably express either YFP-TIA1 (Fig. 2a-2c) or CFP-DCP1a (Fig. 2e); validated markers of PBs and SGs, respectively [reviewed in [29]]. We first confirmed that our YFP-TIA1 "stress" biosensor responded to stress similar to YFP-A3G (see Fig. 1a) by treating cells with 250 μM Ars [30] (Fig. 2a, right panel) or infecting cells with rhinovirus A16 (RVA16), a positive-strand RNA virus we had studied previously[32] and discovered to cause rampant SG formation as early as 4h post-infection (Fig. 2b and Video 3).

Unlike RVA16, neither Vif+ nor Vifxx HIV-1 triggered SG formation in either YFP-TIA1 or YFP-A3G cells over 48h of continuous imaging, a time window sufficient to encompass an entire round of viral replication (Fig. 2c with quantification in 2d). HIV-1

also had no discernible effects on PB number or morphology in CFP-DCP1A biosensor cells; with PB number being remarkable consistent and stable for all individual cells and conditions (typically 6-9 PBs per cell, Fig. 2e with quantification in 2f). Based on these largely negative results, we concluded that despite HIV-1's marked effects on YFP-A3G as shown in Fig. 1, net modulation of PBs or induction of SGs are unlikely to be intrinsic features of the HIV-1 replication cycle.

Because HIV-1 Gag was recently reported to inhibit SG formation[33,34], we also tested the effects of treating HeLa.YFP-A3G or HeLa.YFP-TIA1 biosensor cells with Ars at 31 hpi when NL4-3 Gag expression in HeLa cells is relatively high (*e.g.*, see [31]). Contrary to our expectations, both YFP-A3G and YFP-TIA1 accumulated in SGs in Ars-treated cells infected with either Vif+ or Vifxx viruses (Fig. 2g with quantification in 2h). To localize Gag and genome under these conditions, we again performed combined Gag IF and genome FISH, finding that the bulk of the HIV-1 genome signal co-localized with YFP-A3G in Ars-induced SGs at this time point (Fig. 2i, *gag-pol* FISH). By contrast, the cytoplasmic pool of Gag was largely excluded from these complexes (Fig. 2i, anti-p24).

SGs are induced in response to protein kinase R-mediated phosphorylation of translation initiation factor eIF2a, triggering aggregation of scaffolding proteins that include TIA1, TIAR, and G3BP1 in complex with mRNAs bound to translation initiation factors and polysome-associated proteins [reviewed in [29,35]]. Accordingly, co-localization of YFP-A3G with genomes in SGs could suggest stronger recognition of genomes by YFP-A3G relative to Gag in association with free ribosomes in the cytosol.

HIV-1 RNA genomes but not Gag modulate A3G subcellular mobility; evidence for genome-A3G interactions in the cytosol. So that we could also monitor Gag and genome trafficking dynamics in living HeLa.YFP-A3G cells, we next engineered two-color, HIV-1 genomes that encoded CFP-tagged Gag from a "self-tagging" genome bearing 24 copies of MS2 RNA binding loop (located in the *gag-pol* open reading frame; ORF) and expressing an RFP-tagged MS2 bacteriophage (MS2-RFP) coat protein from the viral *nef* locus (Gag-CFP/MS2-RFP virus, see cartoon depictions in Figs. 3a and 3c). Gag-CFP allowed for single cell measurements of viral late gene expression, with genomes tracked based on their binding to the MS2-RFP protein. Expression of Vif+ or Vifxx Gag-CFP/MS2-RFP viruses recapitulated effects seen during infection with CFP reporter viruses (Figs. 1 and 2); including rapid, Vif-dependent down-regulation of YFP-A3G (decay rate = 25.9% per hour +/- 7.0%; n = 31, Fig. 3b, green, with quantification in Figs. 3e and 3f, Video 4) and, for Vif-deficient (Vifxx) conditions, co-clustering of YFP-A3G, MS2-RFP-tagged genomes, and Gag-CFP to assembly sites at the plasma membrane (Fig. 3d, arrows, Video 5; and see Fig. 4d for an image recorded at higher magnification). We observed Vif-mediated YFP-A3G degradation to occur prior to the onset of virus particle assembly (Fig. 3b, compare 2 h and 3 h time points), consistent with a prior report[36], but at >1h after genomes had populated the cytoplasm (Fig. 3d, compare 1h and 4h time points).

Both prior to and during virus particle assembly, Vifxx genomes and YFP-A3G were co-distributed in a non-localized fashion throughout the cytoplasm, with YFP-A3G but not genome or Gag-CFP accumulating at PBs (Fig. 3d, 2 and 3 h time points post-detection of MS2-RFP). To test if genomes and YFP-A3G were interacting in the fluid compartment,

we performed fluorescence recovery after photobleaching (FRAP) analysis to measure rates of YFP-A3G recovery with or without genomes and in the presence or absence of Gag (Figs. 3g, 3h, and quantification in 3i). Infection with Vifxx HIV-1 mCherry reporter virus reduced rates of YFP-A3G recovery ($t_{1/2}$ = 34.4 s +/- 5.3 s; *n*=8) relative to an uninfected "YFP-A3G alone" control ($t_{1/2}$ = 27.0 s +/- 13.5 s; *n*=14). Interestingly, we also observed incomplete recovery of YFP-A3G at the latest time points in infected cells (~75% recovery compared to nearly 90% for untreated control cells Fig. 3i); suggesting virus-induced immobilization of YFP-A3G [37].

Expression of genomes in the absence of Gag using a "genome only" Vifxx MS2-RFP genome, wherein we mutated the *gag* start codon to abolish Gag synthesis (see Fig. 3g), yielded markedly slower rates of YFP-A3G recovery ($t_{1/2}$ = 70.8 s +/- 27.6 s; *n*=6) relative to both the "YFP-A3G Alone" condition, and a "Gag Only" condition wherein we expressed Gag-mCherry from an mRNA modified to lack 5' and 3' viral regulatory RNA sequences and codon-optimized to further reduce potential contributions of viral *cis*-acting RNA elements located in the *gag* ORF (COGag-mCh; $t_{1/2}$ = 30 s +/- 8.9 s; *n*=7) (Fig. 3i). Taken together, because the expression of genomes but not Gag altered YFP-A3G movements in the cytoplasm based on FRAP analysis, genome-YFP-A3G interactions are likely initiated in the cytoplasm independently of virus particle assembly; and potentially even prior to the onset of Gag synthesis.

Genome-A3G interactions are selective, Gag-independent, and initiated prior to the onset of virus particle assembly. Because FRAP was unable to distinguish between direct or indirect genome-A3G interactions, we next developed a single cell assay to allow

us to measure the strength and specificity of RNA-RBP interactions in the cytoplasm head on; dubbed the In-Cell RNA-Protein Interaction Protocol (IC-IP) (depicted in Fig. 4a). The IC-IP was based on the principle of immobilizing genomes at unnatural sites in the cytoplasm (*e.g.*, membranes or the actin cytoskeleton) using an MS2-based tethering strategy that we have described previously[38]. Should an RBP such as YFP-A3G be strongly associated with the tethered genome, its localization will be also shifted with clear evidence of RNA-RBP co-localization at the unnatural site of tethering.

For genome-A3G IC-IPs, MSL-bearing genomes served as bait for YFP-A3G, as depicted in Fig. 4a. Genome retargeting was achieved by co-expressing "targeter" MS2 coat proteins that were modified to tether MSL-tagged genomes to either membranes (using Src-MS2; bearing a 10 amino-acid membrane targeting signal) or the actin cytoskeleton (using Lifeact-MS2; bearing a 17 amino acid F-actin targeting signal) (Fig. 4b). The Src-MS2 and Lifeact-MS2 targeters were fused to iRFP670 so that we could co-visualize both the targeter and the genome (labelled with the self-tagging MS2-RFP "tracker" protein, see cartoon depiction in Fig. 4c) without experiencing spectral overlap (see Fig. 4d).

Co-expression of two-color Vifxx Gag-CFP/MS2-RFP genomes with the Src-MS2-iRFP or Lifeact-MS2-iRFP targeters caused moderate re-localization of Gag-CFP proteins from the cytosolic pool to intracellular vesicles (Fig. 4d, compare panels iv. and ix.) or F-actin filaments (Fig. 4d, compare panels iv. to xiv.), respectively; consistent with a subset of Gag proteins co-trafficking with its genome substrate in the cytosol (as we have previously shown[38]). Remarkably, however, re-localization of YFP-A3G was more striking, with >50% of the net YFP-A3G per cell fluorescent signal now associated with

intracellular vesicles or F-actin filaments (Fig. 4d, compare panels ii., viii., and xiii., and see YFP-A3G regions-of-interest; ROI; with quantification in 4e and 4f). Consistent with our results from FRAP analyses (Figs. 3g and 3h), a "genome only" bait was sufficient to recruit >50% of YFP-A3G to intracellular vesicles as directed by Src-MS2, suggesting that Gag plays no role in genome-A3G cytosolic interactions (Figs. 5a and 5b). By contrast, a control MSL-bearing mRNA encoding codon-optimized Gag-CFP ("Gag Only") had no effect on YFP-A3G cytoplasmic distribution (Figs. 5c and 5d). Collectively, these results indicated that HIV-1 genome-A3G interactions in the cytoplasm are strong, specific, and occur in the presence or absence of Gag.

A particularly useful feature of the IC-IP is that it could be coupled to video microscopy in order to determine the timing of YFP-A3G-genome interactions timed to the onset of viral gene expression. Live cell imaging of cells co-expressing Src-MS2-iRFP670 with a "Genome Only" RNA bait demonstrated that YFP-A3G was relocalized to vesicles within two hours of first detecting genome expression in the cytoplasm (Fig. 5e, compare 1h and 2h time points, and see Video 6 for additional detail). Accordingly, this experiment indicated that strong genome-A3G interactions are initiated concomitantly with or very soon after genome nuclear export.

Tethering A3G to membranes arrests HIV-1 genome trafficking and reduces virus particle production. We reasoned that if A3G's interactions with genomes were sufficiently strong, then tethering A3G to membranes would, as a corollary, arrest HIV-1 genome mobility in the cytosol and abolish genome trafficking to sites of virus particle assembly. To test this idea, we engineered a "reciprocal" IC-IP experiment (Fig. 6a)

wherein YFP-A3G was modified so that it would bind membranes due to its bearing the same N-terminal Src-derived myristoylation signal we used for our Src-MS2 genome retargeting constructs (Figs. 2b-2e). This fusion protein (Src-YFP-A3G) was co-expressed with two-color (Gag-CFP/MS2-RFP) Vifxx (Fig. 6b) or a CFP-tagged variant (Src-CFP-A3G) co-expressed with one-color (MS2-RFP) "Genome Only" Vifxx genomes (Fig. 6c). As would be anticipated for a strong interaction, Src-FP-A3G expression induced the marked clustering of MS2-RFP-tagged genomes to perinuclear vesicles, with genomes co-localizing with Src-FP-A3G (Figs. 6b and 6c). To address the more relevant scenario of infected cells, we also generated a cell line constitutively expressing Src-YFP-A3G (HeLa.Src-YFP-A3G cells) and infected these cells with a Vifxx reporter virus (Fig. 6d). As expected, we observed genomes (and, to a lesser extent, Gag) co-clustering with Src-YFP-A3G at cytoplasmic vesicles at 24 hpi, detected using combined IF/FISH (Fig. 6d, bottom, white arrows).

We hypothesized that arrest of genome subcellular trafficking due to Src-YFP-A3G expression would reduce Gag synthesis and net virus particle production. Consistent with this hypothesis, co-expression of Src-YFP-A3G or a Src-MS2 control with MSL-tagged 2-color genome (Gag-BFP in this experiment) yielded a dose-dependent reduction to cytosolic Gag level and net efficiency of virus particle release (Fig. 6e). Taken together, these experiments indicated that A3G-genome interactions in the cytosol are sufficiently strong that tethering A3G to membranes can effectively repurpose this protein as an inhibitor of genome trafficking and net virion production.

The presence of genomes promotes more consistent per virion delivery of A3G to sites of virus particle assembly. Combined, the above experiments suggested that A3G has evolved to preferentially recognize one or more HIV-1 genome RNA signatures. However, A3G is encapsidated by Gag into virus particles even in the absence of packageable genomes[17–19]. In an effort to better rationalize prior observations of A3G genome specificity vs. promiscuity, we performed a comparative single virion analysis (SVA) of A3G delivery into virus particles; based on a technique originally pioneered by the Hu and Pathak groups wherein fluorescently-labeled virus-like particles (VLPs) are harvested from HEK293T cells (that produce a greater quantity of particles relative to HeLa) and subjected to sub-micron quantitative multicolor fluorescence imaging to measure relative levels of per particle genome and/or A3G incorporation[39,40] (Fig. 7). For our analysis, we compared per particle levels of YFP-A3G encapsidation for four independent Gag/genome scenarios (depicted in Fig. 7a); “Gag-Only” mRNAs encoding codon-optimized Gag-CFP (COGag-CFP = “Gag-Only”), viral Vif+ or Vifxx 2-color HIV Gag-CFP/MS2-RFP genomes, or mRNAs encoding codon-optimized Gag-CFP wherein the NC RNA-binding domain was replaced by a leucine zipper (ΔNCzip) to abolish Gag-RNA binding (based on [41]). As expected, YFP-A3G packaging was only observed for COGag and the Vifxx HIV-1 conditions (Fig. 7b).

Using SVA, Vif+ and Vifxx viruses exhibited high efficiency MS2-RFP incorporation (~89 and ~88% of Gag-CFP particles scoring positive for MS2-RFP, respectively), very consistent with a prior report of HIV-1 genome packaging efficiency[39]. Vifxx Gag-CFP/MS2-RFP particles exhibited a similar frequency of YFP-A3G incorporation (86% of total Gag-CFP particles) (Fig. 7c and quantification in 7d). However, for “Gag-Only”

(COGag-CFP) particles, the frequency of detectable YFP-A3G incorporation was lower (57% efficiency), intermediate to Vifxx HIV-1 vs. the ΔNCzip "no-RNA" negative control (Fig. 7c and quantification in 7d). COGag particles also exhibited reduced per virion levels of YFP-A3G fluorescence when compared to full-length, Vifxx HIV (Fig. 7c and quantification in 7e). In sum, these data indicated that, although genomes are not essential for YFP-A3G delivery to virus particles, selective genome-A3G interactions promote a more consistent and more enriched per virion delivery of A3G to virus particle assembly sites.

DISCUSSION

Herein we studied the HIV-1 life cycle from the host cell perspective, combining several complementary live cell imaging approaches with functional assays to characterize the coordinated behaviors A3G, PB or SG proteins, and viral elements (Gag and genome) over an entire round of viral replication (summarized in Fig. S1).

Our YFP-A3G biosensor allowed for indirect measurements of HIV-1 replication kinetics in single cells and exposed A3G behaviors including; (1) that Vif-mediated A3G degradation occurs from all subcellular pools simultaneously (Fig. 1d and Movie 1); (2) that A3G suppression by Vif is remarkably stable and maintained over the entire late phase of infection (lasting hours to days, see Figs. 1d, Movie 1, and 1e); and (3) that A3G degradation is completed prior to the onset of virus particle assembly (very consistent with prior report from Holmes *et al*.,[36] but shown here to be after genome nuclear export) (Fig. 3b). In the absence of Vif, we could also monitor virus particle assembly, observing large quantities of YFP-A3G being re-localized from the cytoplasm to the plasma membrane during this process (Fig. 1f and Video 2). Taken together, on a technical level there should be great utility in the general strategy of tracking RBP biosensors to detect virus replication dynamics and study host cell responses (*e.g.*, see also RVA16-induced stress in Fig. 2b). Moreover, now validated, HeLa.YFP-A3G cells should serve as useful multivariate reporter system for further dissection of the viral and host machineries governing A3G degradation and packaging.

Despite HIV-1's marked effects on YFP-A3G behaviors, we observed little to no discernible effects of HIV-1 on SGs or PBs monitored using our YFP-TIA1 or CFP-DCP1A biosensors, with or without Vif expression (Fig. 2). These movies reinforce that

345 modulation of PB number or architecture or SG induction is unlikely to be an intrinsic
346 feature of the HIV-1 life cycle[27,28]. Overall, the underlying significance of A3G's localization
347 to PBs and SGs remains is unknown; but predicted to spatially coupled A3G to RNP
348 complexes with active roles in viral mRNA surveillance (*i.e.*, PBs are sites miRNA-
349 dependent mRNA decay and SGs can suppress viral translation)[23,24,26]. In this context,
350 we speculate that all successful retroviruses and endogenous elements must adapt to
351 subvert, suppress, or avoid PB- or SG-associated activities. Indeed, HIV-1[42,43], other
352 retroviruses[44,45], and endogenous retroelements including LINEs[46] and yeast Ty
353 elements[47] are thought to exploit non-membranous RNP complexes related to PBs/SGs
354 in order to compartmentalize activities including mRNA translation and genome
355 packaging. Regarding suppression, intriguing recent work from Mouland and colleagues
356 has shown HIV-1 to actively inhibit SG formation, proposed to reduce the potential for
357 stress signaling triggered by Gag NC interacting with host RNA species[33,34]. While we did
358 not observe overt SG suppression in this study (Figs. 2g-i), the dynamics of this process
359 warrant additional investigation and it seems reasonable to posit that retroviruses prevent
360 SG formation to promote a fluid flow of genomes from the nucleus to polysomes and then
361 on to capsid assembly sites. Overall, however, our data support the notion that HIV-1's
362 general *modus operandi* is to largely avoid association with visible PBs or induction of
363 SGs.

364 At a more molecular level, our imaging assays also suggest that A3G is able to
365 selectively compete for genome binding in the cytosol. First, HIV-1 genomes but not Gag
366 rapidly accumulated at YFP-A3G-enriched SGs in infected cells after Ars treatment (Fig
367 2i). Second, based on FRAP analysis, the presence of genomes, but not Gag, reduces

A3G mobility in the cytoplasm (Fig. 3g and 3h). Third, and most convincingly, our IC-IP experiments demonstrated that >50% of the cytosolic YFP-A3G is recruited to membranes or F-actin by Src- or Lifeact-MS2-tethered genomes, respectively, (Fig. 4f); effects that were far less evident for Gag-CFP; not observed in the absence of genomes (Fig. 5d); and detected soon if not immediately after genome nuclear export (Fig. 5e). As to *why* A3G competes for genome binding, single virion analyses (Fig. 7) revealed an ~90% frequency of A3G incorporation into genome-containing virions relative to "Gag-only" particles wherein the frequency of A3G incorporation was less than 60%. This result suggests to us that, although A3G-RNA binding is, overall, relatively promiscuous[19], it has evolved to preferentially target genomes in a way that ensures consistent and efficient delivery to virions, largely consistent with a model recently proposed by Bieniasz and colleagues wherein Gag and A3G are adapted to compete for similar RNA sequences[20]. In this way, A3G maximizes its antiviral potential and thus necessitated evolution of the Vif antagonist. Endeavors to further delineate the relevant protein constituents of A3G-genome "surveillance" complexes, and to determine whether or not A3G exhibits differential detection of genomes destined for packaging vs. translation (as *gag-pol* mRNAs), are ongoing.

To summarize, our studies reinforce that the core, essential nature of genome trafficking in the cytosol is diffusion in dynamic association with RNP complexes, with some proteins (*e.g.*, A3G) more strongly associated with genomes than others. While we have yet to define the RNA signature(s) that specify genome detection by A3G, our observations may be informative in the context of recent CLIP-seq studies demonstrating A3G's RNA-binding preference to be relatively sequence non-specific[19,20] coupled to

391 compelling recent work showing that HIV-1 genomes are selectively enriched in selective
392 post-transcriptional regulatory marks including N_6 methyladenosine (m6a)[48–50], 5-
393 methylcytosine (m5c), and 2'O-methylation[51]. Artificially tethering A3G to membranes
394 restricts HIV-1 genome trafficking and virus particle assembly (Fig. 6). Based on these
395 effects, we predict it will be feasible to design inhibitory molecules or biologicals capable
396 of achieving similar strong, selective inhibition of HIV-1 RNA trafficking, translation, and
397 genome packaging in the context of antiviral strategies.

ACKNOWLEDGEMENTS

We thank Randall Massey at the University of Wisconsin SMPH Electron Microscopy Facility for assistance with EM sample preparation. We are grateful to Michael Malim (King's College London), Chad Swanson, (King's College London), and Sarah Gallois-Montbrun (Institut Cochin) for plasmid reagents and advice. The following reagent was obtained through the NIH AIDS Reagent Program, Division of AIDS, NIAID, NIH: HIV-1 p24 hybridoma (183-H12-5C) (from Bruce Chesebro)[52]. We thank Kelly Watters, Marchel Hill, and Ann Palmenberg for RVA16[32]. This study was supported by NIH grants RO1AI110221 and U54AI150470; the Wisconsin Partnership Program New Investigator Program (ID 2830); the Greater Milwaukee Foundation's Shaw Scientist Program; and the UW-Madison UW2020 Program to N.M.S. J.T.B. was supported by National Science Foundation Graduate Research Fellow Program grant DGE-1256259 and both a Research Competition Award and a Dissertation Completion Fellowship from the UW—Madison office of the Vice Chancellor of Research and Graduate Education. Any opinions, findings, and conclusions or recommendations expressed in this material are those of the authors and do not necessarily reflect the views of the National Science Foundation. E.L.E. III received support from NIH training grant CA009135 and an Advance Opportunity Fellowship from the UW-Madison SciMed/GRS program. B.E.B. was supported by National Science Foundation Graduate Research Fellow Program grant DGE-1256259 and NIH training grant GM008349. S.L.F. received support from a UW-Madison Hilldale Undergraduate Research Fellowship.

AUTHOR CONTRIBUTIONS:

JTB and NMS conceived the project, designed reagents, and established methods. JTB carried out all experiments and wrote the first version of the manuscript. ELE, BEB, SLF, LES, and AEB contributed reagents and generated preliminary data. JTB, ELE, and NMS processed and analyzed data. All authors contributed to the final revised manuscript and approved submission.

METHODS

Cell culture, plasmids, and stable cell lines. Human HeLa and HEK293T cell lines (obtained from ATCC) were cultured in DMEM (Sigma-Aldrich) supplemented with 10% fetal bovine serum (heat-inactivated, filter-sterilized), 1% L-glutamine, and 1% penicillin-streptomycin. HeLa.YFP-A3G, HEK293T.YFP-A3G, HeLa.Src-YFP-A3G, HeLa.YFP-TIA1, and HeLa.CFP-DCP1a were generated as previously described[38]. Briefly, YFP-A3G, Src-YFP-A3G, YFP-TIA1, and CFP-DCP1a cDNA[24] were inserted into a MIGR1-derived retroviral vector (pCMS28) upstream of sequence encoding an internal ribosome entry site (IRES) and a second reading frame encoding Puromycin-N-acetyltransferase[48]. High performance clones were selected by limiting dilution and maintained in 2μg/mL puromycin. YFP, YFP-A3G, and Src-YFP-A3G as well as CFP versions of construct were also generated using the pcDNA3.1 transient expression vector backbone. HIV-1 reporter virus plasmids were derived from the pNL4-3 molecular clone[53] bearing inactivating mutations in *env*, *vpr*, and expressing a green fluorescent protein (GFP) reporter from the *nef* locus (E-R-/GFP)[54]; with the GFP reporter replaced with either cerulean fluorescent protein (CFP) or mCherry (mCh). Vif-minus HIV-1 reporter virus plasmids (Vifxx CFP and Vifxx mCherry) were generated by changing *vif* codons 26 and 27 to stop codons[55] using overlapping PCR and inserted into Vif+ CFP and Vif+ mCherry plasmids. Two-color fluorescent HIV-1 reporter viruses (Gag-CFP/MS2-RFP) were generated by replacing the *gag* reading frame in Vif+ and Vifxx CFP reporter viruses with *gag-CFP* just upstream of a cassette encoding 24 copies of the MS2 bacteriophage RNA stem loop (MSL, a kind gift of Robert Singer, Albert Einstein University, New York, NY, USA)[56], and then subsequently replacing CFP with sequence encoding the MS2 coat protein fused to

mApple or mCherry and bearing an SV40 nuclear localization signal (MS2-RFP). Gag was also fused to mTagBFP2 for select experiments (*e.g.*, Fig. 6e) in order to avoid CFP/YFP cross-detection when immunoblotting for Src-YFP-A3G. Mutated versions of full-length HIV-1 were generated using overlapping PCR as previously described[38]. Src-MS2-CFP, Src-MS2-RFP, and Src-MS2-iRFP targeting constructs encoding an amino-terminal membrane targeting signal derived from the Src kinase (MGSSKSKPKD) were generated by overlapping PCR and subcloned into pcDNA3.1. mTurquoise2 (CFP) and mApple (RFP) were gifts of Michael Davidson (Addgene # 54843 and 54747, respectively). iRFP670 cDNA[57] was amplified from the ColorfulCell expression plasmid, a gift of Pierre Neveu (Addgene plasmid # 62449)[58]. mTagBFP2[59] was a gift of Michal Davidson (Addgene plasmid # 55302).

Retroviral assembly and infectivity assays. Cells at 30-40% confluency were transfected with 2µg DNA in six well plates using polyethylenimine (PEI; #23966, Polysciences Inc.). pcDNA3.1 or pBlueScript were used as empty vector controls. Culture media were replaced at 24 hours post-transfection and cell lysates and supernatants were harvested for immunoblot analysis at 48 hours as previously described[60](Sherer et al. 2011). Briefly, 1mL of harvested culture supernatant was filtered, underlaid with 20% sucrose (w/v) in PBS, subjected to centrifugation at >21,000g for two hours at 4ºC, and viral pellets were resuspended in 35µL dissociation buffer (62.5 mM Tris-HCl, pH 6.8, 10% glycerol, 2% sodium dodecyl sulfate [SDS], 5% β-mercaptoethanol). Cells were harvested in 500µL radioimmunoprecipitation assay (RIPA) lysis buffer (10 mM Tris-HCl, pH 7.5, 150 mM NaCl, 1 mM EDTA, 0.1% SDS, 1% Triton X-100, 1% sodium

deoxycholate), homogenized by passage through a 26G needle, subjected to centrifugation at 1,500g for 20 minutes at 4ºC, and liquid supernatant fraction was combined 1:1 with 2X dissociation buffer. Proteins were resolved by sodium dodecyl sulfate-polyacrylamide gel electrophoresis (SDS-PAGE) and transferred to 0.2 µm nitrocellulose membranes. Gag was detected using a mouse monoclonal antibody recognizing HIV-1 capsid/p24 (183-H12-5C; 1:1000 dilution) from Dr. Bruce Chesebro and obtained from the NIH AIDS Research and Reference Reagent Program (Bethesda, MD, USA)[52] and anti-mouse secondary antibodies conjugated to an infrared fluorophore (IRDye680LT, 1:10000 dilution, Li-Cor Biosciences) for quantitative immunoblotting. As loading controls, heat shock protein 90A/B (HSP90) was detected using a rabbit polyclonal antibody (H-114, 1:2500 dilution, Santa Cruz Biotechnology, Santa Cruz, CA, USA) or glyceraldehyde 3-phosphate dehydrogenase (GAPDH) was detected using a mouse monoclonal antibody (6C5, 1:2500 dilution, Santa Cruz Biotechnology) and anti-rabbit or anti-mouse secondary secondary antibodies conjugated to an infrared fluorophore (IRDye800CW, 1:7500 dilution, Li-Cor Biosciences). YFP-containing proteins (*e.g.*, YFP-A3G) were detected using a rabbit polyclonal antibody recognizing GFP (FL sc-8334, 1:1000 dilution, Santa Cruz Biotechnology) and anti-rabbit secondary antibodies conjugated to an infrared fluorophore (IRDye800CW). For infectivity assays, supernatants containing single-round infectious HIV-1 virions (pseudo-typed with VSV-G) were filtered and then added to target HeLa cells in the presence of 10µg/mL polybrene. Approximately 36 hours later, target HeLa cells were scanned using a BioTek Cytation5 to detect reporter CFP (455nm/510nm excitation/emission filter) expression following infection.

Microscopy, immunofluorescence, and FISH. Cells were plated in 24-well glass-bottom plates (Eppendorf) or 8-well microslides (IBIDI) and transfected using PEI or infected with HIV-1 reporter viruses. Transfection mixes contained 1µg (24-well) or 333ng (IBIDI) total plasmid DNA, respectively. Infections were performed with VSV-G pseudo-typed HIV-1 reporter viruses produced in HEK293T cells and titered on HeLa cells to determine MOI of 0.5-1, thereby ensuring that 33-66% of the cells would be infected per experiment. Fixed-cell experiments were performed on a Nikon Ti-Eclipse inverted wide-field microscope (Nikon Corporation, Melville, NY, USA) using a 100x Plan Apo oil objective (numerical aperture [NA], 1.45). Transfected cells were fixed 24 – 32 hours post-transfection and infected cells were fixed 42 hours post-infection using 4% paraformaldehyde. If treated with 250 µM sodium arsenite (Sigma-Aldrich), drug or an equivalent volume of dimethyl sulfoxide were added to cell culture wells at approximately one hour prior to fixation and returned to incubation at 37ºC. Live-cell imaging experiments were also performed on a Nikon Ti-Eclipse inverted wide-field microscope using a 20x Plan Apo objective lens (NA, 0.75) with images acquired every 60 minutes (except where otherwise indicated) over a time course of 16 to 90 hours. Images were acquired using an ORCA-Flash4.0 CMOS camera (Hammatsu Photonics) and the following excitation/emission filter sets (nanometer ranges): BFP (402/455), CFP (430/470), YFP (510/535), mApple (555/605), mCherry (572/632), and iRFP (645/705). All images were processed and analyzed using FIJI/ImageJ2.

For fixed-cell experiments using FISH, cells were plated as described as above and previously[38]. At 42 hours post-infection or after 24 hours plated (for uninfected cells),

cells were washed, fixed in 4% formaldehyde, and permeabilized in 70% ethanol for at least 4 hours at 4ºC. Custom Stellaris FISH probes were designed to recognize NL4-3 HIV-1 *gag-pol* reading frame nucleotides 386-4456 using the Stellaris RNA FISH Probe Designer 4.1 (Biosearch Technologies, Inc.) available online. To detect *yfp* mRNAs, we used a DesignReady Probe set specific to eGFP. Both probe sets were labeled with CAL Fluor Red 590 Dye (Biosearch Technologies, Inc.). Samples were hybridized with the *gag/gag-pol* probe set according to the manufacturer's instructions available online. Simultaneous immunofluorescence to detect Gag used a mouse monoclonal antibody specific to p24 (#24-2, a gift from Dr. Michael Malim). Imaging experiments were performed as describe above on a Nikon Ti-Eclipse inverted wide-field microscope using a 100x Plan Apo objective lens.

FRAP experiments were performed using a Nikon Ti-Eclipse inverted A1R+ resonant/galvano hybrid confocal line-scanning microscope. Images were captured using a 20x Plan Apo objective lens (NA, 0.75) and a GaAsP multi-detector for 488 and 560nm channels. YFP-A3G was imaged using the 488nm laser at a low arbitrary intensity and photobleached using the laser's maximum intensity. MS2-RFP and COGag-mCherry were imaged using the 560nm laser at a low arbitrary intensity. Cells were maintained in an environmental chamber (Pathology Devices, Inc.) at 37ºC, 5% CO_2, and 50% humidity. Cells were imaged every 30 seconds for 4 frames prior to photobleaching (3 rapid ablations of cytoplasmic ROIs 10µm in diameter) followed by imaging every 5 seconds for a minute, 15 seconds for four minutes, and 30 seconds for 5 minutes. This time frame was sufficient for fluorescence recovery to reach a plateau. FRAP analysis was performed

using the FIJI plugin FRAP Profiler[61] that adjusts for incidental field photobleaching outside the ROI.

Single virion analyses (SVA) were performed as previously described[39]. Virus particles were produced as described above for western blotting in HEK293T.YFP-A3G cells to maintain consistent levels of YFP-A3G. Filtered culture supernatants (750µL) were purified by sucrose centrifugation as described above and resuspended in 100µL 1x PBS (Sigma-Aldrich). 24-well plates were pre-coated with 2% FBS diluted in 1x PBS for at least 30 minutes, this solution was removed, and the resuspended concentrated virus particles were added to wells. Images were acquired on a Nikon Ti-Eclipse inverted wide-field microscope using a 100x Plan Apo objective lens (NA, 1.45). These images were processed and analyzed using Analyze Particles plugin in FIJI/ImageJ2[62].

Thin-section electron microscopy. HeLa.YFP-A3G were infected with Vif+ CFP or Vifxx CFP HIV-1 viruses and fixed at 48 hours for chemical processing as previously described[63]. Samples were sectioned into 100nm slices and with sections collected on copper thin-bar grids. Sections were observed with a Phillips CM120 transmission electron microscope, and images were collected with a MegaView III (Olympus-SIS, Lakewood, CO, USA) side-mounted digital camera. All images were processed and analyzed using FIJI/ImageJ2[62].

Statistics. For assembly assays (Figs. 1b and 6e), results were obtained from three biological replicates as defined as cells plated in six well plates transfected and processed on separate days. Graphs plot the mean value with error bars representing the standard

563 deviation of the mean with the exception of Fig. 7e, a violin plot showing all data points
564 with the mean (solid line) and quartiles (dashed lines) indicated. All statistical
565 comparisons were carried out using the two-tailed Student's *t* test and performed using
566 Microsoft Excel or Graphpad Prism.

REFERENCES

1. Bolinger, C. & Boris-Lawrie, K. Mechanisms employed by retroviruses to exploit host factors for translational control of a complicated proteome. *Retrovirology* **6**, 8 (2009).
2. Cochrane, A. W., McNally, M. T. & Mouland, A. J. The retrovirus RNA trafficking granule: from birth to maturity. *Retrovirology* **3**, 18 (2006).
3. Karn, J. & Stoltzfus, C. M. Transcriptional and posttranscriptional regulation of HIV-1 gene expression. *Cold Spring Harb. Perspect. Med.* **2**, a006916 (2012).
4. Swanson, C. M. & Malim, M. H. Retrovirus RNA trafficking: from chromatin to invasive genomes. *Traffic Cph. Den.* **7**, 1440–1450 (2006).
5. Harris, R. S. *et al.* DNA deamination mediates innate immunity to retroviral infection. *Cell* **113**, 803–809 (2003).
6. Malim, M. H. APOBEC proteins and intrinsic resistance to HIV-1 infection. *Philos. Trans. R. Soc. Lond. B. Biol. Sci.* **364**, 675–687 (2009).
7. Refsland, E. W. & Harris, R. S. The APOBEC3 family of retroelement restriction factors. *Curr. Top. Microbiol. Immunol.* **371**, 1–27 (2013).
8. Sheehy, A. M., Gaddis, N. C., Choi, J. D. & Malim, M. H. Isolation of a human gene that inhibits HIV-1 infection and is suppressed by the viral Vif protein. *Nature* **418**, 646–650 (2002).
9. Mariani, R. *et al.* Species-specific exclusion of APOBEC3G from HIV-1 virions by Vif. *Cell* **114**, 21–31 (2003).
10. Sheehy, A. M., Gaddis, N. C. & Malim, M. H. The antiretroviral enzyme APOBEC3G is degraded by the proteasome in response to HIV-1 Vif. *Nat. Med.* **9**, 1404–1407 (2003).
11. Stopak, K., de Noronha, C., Yonemoto, W. & Greene, W. C. HIV-1 Vif blocks the antiviral activity of APOBEC3G by impairing both its translation and intracellular stability. *Mol. Cell* **12**, 591–601 (2003).
12. Freed, E. O. HIV-1 assembly, release and maturation. *Nat. Rev. Microbiol.* **13**, 484–496 (2015).
13. Eckwahl, M. J. *et al.* Analysis of the human immunodeficiency virus-1 RNA packageome. *RNA N. Y. N* **22**, 1228–1238 (2016).
14. Rulli, S. J. *et al.* Selective and nonselective packaging of cellular RNAs in retrovirus particles. *J. Virol.* **81**, 6623–6631 (2007).
15. Zennou, V., Perez-Caballero, D., Göttlinger, H. & Bieniasz, P. D. APOBEC3G incorporation into human immunodeficiency virus type 1 particles. *J. Virol.* **78**, 12058–12061 (2004).
16. Khan, M. A. *et al.* Analysis of the contribution of cellular and viral RNA to the packaging of APOBEC3G into HIV-1 virions. *Retrovirology* **4**, 48 (2007).
17. Cen, S. *et al.* The interaction between HIV-1 Gag and APOBEC3G. *J. Biol. Chem.* **279**, 33177–33184 (2004).
18. Alce, T. M. & Popik, W. APOBEC3G is incorporated into virus-like particles by a direct interaction with HIV-1 Gag nucleocapsid protein. *J. Biol. Chem.* **279**, 34083–34086 (2004).
19. Apolonia, L. *et al.* Promiscuous RNA binding ensures effective encapsidation of APOBEC3 proteins by HIV-1. *PLoS Pathog.* **11**, e1004609 (2015).
20. York, A., Kutluay, S. B., Errando, M. & Bieniasz, P. D. The RNA Binding Specificity

of Human APOBEC3 Proteins Resembles That of HIV-1 Nucleocapsid. *PLoS Pathog.* **12**, e1005833 (2016).
21. Svarovskaia, E. S. *et al.* Human apolipoprotein B mRNA-editing enzyme-catalytic polypeptide-like 3G (APOBEC3G) is incorporated into HIV-1 virions through interactions with viral and nonviral RNAs. *J. Biol. Chem.* **279**, 35822–35828 (2004).
22. Gallois-Montbrun, S. *et al.* Comparison of cellular ribonucleoprotein complexes associated with the APOBEC3F and APOBEC3G antiviral proteins. *J. Virol.* **82**, 5636–5642 (2008).
23. Wichroski, M. J., Robb, G. B. & Rana, T. M. Human retroviral host restriction factors APOBEC3G and APOBEC3F localize to mRNA processing bodies. *PLoS Pathog.* **2**, e41 (2006).
24. Gallois-Montbrun, S. *et al.* Antiviral protein APOBEC3G localizes to ribonucleoprotein complexes found in P bodies and stress granules. *J. Virol.* **81**, 2165–2178 (2007).
25. Chable-Bessia, C. *et al.* Suppression of HIV-1 replication by microRNA effectors. *Retrovirology* **6**, 26 (2009).
26. Nathans, R. *et al.* Cellular microRNA and P bodies modulate host-HIV-1 interactions. *Mol. Cell* **34**, 696–709 (2009).
27. Izumi, T. *et al.* Mov10 and APOBEC3G localization to processing bodies is not required for virion incorporation and antiviral activity. *J. Virol.* **87**, 11047–11062 (2013).
28. Phalora, P. K., Sherer, N. M., Wolinsky, S. M., Swanson, C. M. & Malim, M. H. HIV-1 replication and APOBEC3 antiviral activity are not regulated by P bodies. *J. Virol.* **86**, 11712–11724 (2012).
29. Ivanov, P., Kedersha, N. & Anderson, P. Stress Granules and Processing Bodies in Translational Control. *Cold Spring Harb. Perspect. Biol.* **11**, (2019).
30. Kedersha, N. *et al.* Dynamic shuttling of TIA-1 accompanies the recruitment of mRNA to mammalian stress granules. *J. Cell Biol.* **151**, 1257–1268 (2000).
31. Evans, E. L., Becker, J. T., Fricke, S. L., Patel, K. & Sherer, N. M. HIV-1 Vif's Capacity To Manipulate the Cell Cycle Is Species Specific. *J. Virol.* **92**, (2018).
32. Watters, K. *et al.* Differential Disruption of Nucleocytoplasmic Trafficking Pathways by Rhinovirus 2A Proteases. *J. Virol.* **91**, (2017).
33. Cinti, A., Le Sage, V., Ghanem, M. & Mouland, A. J. HIV-1 Gag Blocks Selenite-Induced Stress Granule Assembly by Altering the mRNA Cap-Binding Complex. *mBio* **7**, e00329 (2016).
34. Valiente-Echeverría, F. *et al.* eEF2 and Ras-GAP SH3 domain-binding protein (G3BP1) modulate stress granule assembly during HIV-1 infection. *Nat. Commun.* **5**, 4819 (2014).
35. Protter, D. S. W. & Parker, R. Principles and Properties of Stress Granules. *Trends Cell Biol.* **26**, 668–679 (2016).
36. Holmes, M., Zhang, F. & Bieniasz, P. D. Single-Cell and Single-Cycle Analysis of HIV-1 Replication. *PLoS Pathog.* **11**, e1004961 (2015).
37. Ishikawa-Ankerhold, H. C., Ankerhold, R. & Drummen, G. P. C. Advanced fluorescence microscopy techniques--FRAP, FLIP, FLAP, FRET and FLIM. *Mol. Basel Switz.* **17**, 4047–4132 (2012).
38. Becker, J. T. & Sherer, N. M. Subcellular Localization of HIV-1 gag-pol mRNAs

Regulates Sites of Virion Assembly. *J. Virol.* **91**, (2017).
39. Chen, J. *et al.* High efficiency of HIV-1 genomic RNA packaging and heterozygote formation revealed by single virion analysis. *Proc. Natl. Acad. Sci. U. S. A.* **106**, 13535–13540 (2009).
40. Desimmie, B. A. *et al.* APOBEC3 proteins can copackage and comutate HIV-1 genomes. *Nucleic Acids Res.* **44**, 7848–7865 (2016).
41. Accola, M. A., Strack, B. & Göttlinger, H. G. Efficient particle production by minimal Gag constructs which retain the carboxy-terminal domain of human immunodeficiency virus type 1 capsid-p2 and a late assembly domain. *J. Virol.* **74**, 5395–5402 (2000).
42. Reed, J. C. *et al.* HIV-1 Gag co-opts a cellular complex containing DDX6, a helicase that facilitates capsid assembly. *J. Cell Biol.* **198**, 439–456 (2012).
43. Barajas, B. C. *et al.* Identifying the assembly intermediate in which Gag first associates with unspliced HIV-1 RNA suggests a novel model for HIV-1 RNA packaging. *PLoS Pathog.* **14**, e1006977 (2018).
44. Soto-Rifo, R. *et al.* HIV-2 genomic RNA accumulates in stress granules in the absence of active translation. *Nucleic Acids Res.* **42**, 12861–12875 (2014).
45. Bann, D. V., Beyer, A. R. & Parent, L. J. A murine retrovirus co-Opts YB-1, a translational regulator and stress granule-associated protein, to facilitate virus assembly. *J. Virol.* **88**, 4434–4450 (2014).
46. Goodier, J. L., Zhang, L., Vetter, M. R. & Kazazian, H. H. LINE-1 ORF1 protein localizes in stress granules with other RNA-binding proteins, including components of RNA interference RNA-induced silencing complex. *Mol. Cell. Biol.* **27**, 6469–6483 (2007).
47. Larsen, L. S. Z. *et al.* Ty3 nucleocapsid controls localization of particle assembly. *J. Virol.* **82**, 2501–2514 (2008).
48. Kennedy, E. M. *et al.* Posttranscriptional m(6)A Editing of HIV-1 mRNAs Enhances Viral Gene Expression. *Cell Host Microbe* **19**, 675–685 (2016).
49. Lichinchi, G. *et al.* Dynamics of the human and viral m(6)A RNA methylomes during HIV-1 infection of T cells. *Nat. Microbiol.* **1**, 16011 (2016).
50. Tirumuru, N. *et al.* N(6)-methyladenosine of HIV-1 RNA regulates viral infection and HIV-1 Gag protein expression. *eLife* **5**, (2016).
51. Courtney, D. G. *et al.* Epitranscriptomic Addition of m5C to HIV-1 Transcripts Regulates Viral Gene Expression. *Cell Host Microbe* **26**, 217-227.e6 (2019).
52. Chesebro, B., Wehrly, K., Nishio, J. & Perryman, S. Macrophage-tropic human immunodeficiency virus isolates from different patients exhibit unusual V3 envelope sequence homogeneity in comparison with T-cell-tropic isolates: definition of critical amino acids involved in cell tropism. *J. Virol.* **66**, 6547–6554 (1992).
53. Adachi, A. *et al.* Production of acquired immunodeficiency syndrome-associated retrovirus in human and nonhuman cells transfected with an infectious molecular clone. *J. Virol.* **59**, 284–291 (1986).
54. Connor, R. I., Chen, B. K., Choe, S. & Landau, N. R. Vpr is required for efficient replication of human immunodeficiency virus type-1 in mononuclear phagocytes. *Virology* **206**, 935–944 (1995).
55. Simon, J. H. *et al.* The regulation of primate immunodeficiency virus infectivity by Vif is cell species restricted: a role for Vif in determining virus host range and cross-

704 species transmission. *EMBO J.* **17**, 1259–1267 (1998).
705 56. Femino, A. M., Fay, F. S., Fogarty, K. & Singer, R. H. Visualization of single RNA
706 transcripts in situ. *Science* **280**, 585–590 (1998).
707 57. Shcherbakova, D. M. & Verkhusha, V. V. Near-infrared fluorescent proteins for
708 multicolor in vivo imaging. *Nat. Methods* **10**, 751–754 (2013).
709 58. Sladitschek, H. L. & Neveu, P. A. MXS-Chaining: A Highly Efficient Cloning Platform
710 for Imaging and Flow Cytometry Approaches in Mammalian Systems. *PloS One* **10**,
711 e0124958 (2015).
712 59. Subach, O. M., Cranfill, P. J., Davidson, M. W. & Verkhusha, V. V. An enhanced
713 monomeric blue fluorescent protein with the high chemical stability of the
714 chromophore. *PloS One* **6**, e28674 (2011).
715 60. Sherer, N. M. *et al.* Evolution of a species-specific determinant within human CRM1
716 that regulates the post-transcriptional phases of HIV-1 replication. *PLoS Pathog.* **7**,
717 e1002395 (2011).
718 61. Hardin, J. Imaging embryonic morphogenesis in C. elegans. *Methods Cell Biol.* **106**,
719 377–412 (2011).
720 62. Schindelin, J. *et al.* Fiji: an open-source platform for biological-image analysis. *Nat.*
721 *Methods* **9**, 676–682 (2012).
722 63. Garcia-Miranda, P. *et al.* Stability of HIV Frameshift Site RNA Correlates with
723 Frameshift Efficiency and Decreased Virus Infectivity. *J. Virol.* **90**, 6906–6917
724 (2016).

FIGURE LEGENDS

Fig. 1. Tracking the HIV-1 replication cycle using a YFP-A3G biosensor cell line. a HeLa.YFP-A3G cells showing diffuse and punctate (processing bodies, PB, white arrows) distribution of YFP-A3G at steady-state (left) and accumulation into stress granules (SGs, magenta arrows) following arsenite treatment (right, Ars). **b** Schematic of Vif-competent (Vif+) or deficient (Vifxx) HIV-1 NL4-3 Env-, Vpr-, expressing CFP as a reporter of infection. **c** Single-round infection confirms YFP-A3G dependent restriction of HIV-1 in the absence of Vif. 293T.YFP-A3G cells were transfected with the indicated HIV-1 reporter viruses with or without co-expression of a plasmid encoding Vif-mCherry. Cells and virus particles (*n*=3) were harvested at 48 h post-transfection and analyzed by quantitative immunoblot using anti-$p24_{Gag}$, anti-YFP, and anti-HSP90 (loading control) antisera. **d** Representative images from long-term time-lapse imaging showing degradation of YFP-A3G upon HIV-1 Vif+ CFP infection and eventual Vif-dependent G2/M arrest. **e** Quantification of movies (IntDen) represented in d (Vif+, solid lines) and **f** (Vifxx, dashed lines). Cells from 3 independent experiments (*n*=33) with ≥16 hours per cell (1 image/hour). **f** Representative images from long-term time-lapse imaging of YFP-A3G upon HIV-1 Vifxx CFP infection. Magenta boxes highlight zoomed regions of interest (ROIs) shown below and white arrows highlight YFP-A3G clustering at PM. **g** Fixed cell images show Gag and *gagpol* mRNA (viral RNA genomes) accumulating with YFP-A3G at cell periphery. White arrows highlight cell-peripheral clusters of YFP-A3G, Gag, and genome. **h** TSEM images showing virus particles clustering in the extracellular space after budding from HeLa.YFP-A3G cells infected with either Vif+ or Vifxx viruses. All scale

bars in fluorescent images = 10μm and in TSEM = 100nm. Error bars represent standard deviation of the mean.

Fig. 2. HIV-1 infection has little to no impact on P-bodies or stress granules. **a** HeLa.YFP-TIA1 cells showing steady-state distribution (vehicle, left) and accumulation into SGs (magenta arrows) following arsenite treatment (right, Ars). **b** Representative images of time-lapse imaging showing induction of SGs during infection by RVA16 (MOI=10). **c** Time-lapse images showing no effect on YFP-TIA1 distribution following Vifxx CFP infection, quantified in **d** for >400 HeLa.YFP-A3G (black bars) and HeLa.YFP-TIA1 (gray bars) cells per condition, combined from three independent experiments. **e** Time-lapse images showing no effect on CFP-DCP1a following Vifxx mCh infection, quantified in **f** for 30 cells from 3 movies at ~18 hpi (YFP-A3G, black bars; CFP-DCP1a, white bars). **g** HeLa.YFP-A3G infected with Vifxx CFP and treated with Ars to induce SGs at 24 hpi and quantified in **h** for at least 100 infected cells from three independent experiments. Magenta arrows highlight SGs present in infected cells. **i** Simultaneous FISH/IF to detect *gagpol* mRNA and Gag show HIV RNA genomes accumulating in SGs in HIV infected cells following Ars treatment. Magenta arrows highlight SGs present in infected cells. All scale bars in fluorescent images = 10μm. Error bars represent standard deviation of the mean.

Fig. 3. HIV-1 RNA genomes but not Gag regulate A3G subcellular localization. a and c Schematic Vif+ and Vifxx two-color self-tagging virus encoding Gag-CFP, 24xMSL, and MS2-RFP. **b** and **d** Time-lapse images of cells expressing Vif+ and Vifxx two-color HIV

770 constructs showing nuclear export of MS2-RFP tagged genomes, YFP-A3G degradation
771 (**b,** Vif+) or localization with MS2-RFP (**d,** Vifxx), and Gag-CFP expression and
772 accumulation into virus particles at the PM (white arrows). **e** and **f** Quantification of YFP-
773 A3G degradation and MS2-RFP cytoplasmic accumulation (**e**) and Gag-CFP expression
774 (**f**) during expressing of Vif+ two-color HIV construct. Cells (*n*=31) from three independent
775 experiments wherein individual cells that could be tracked for at least 17 h (1 image/hour).
776 Black lines highlight the ~3 h window of YFP-A3G degradation. T=0 represents onset of
777 MS2-RFP expression. **g** Schematic of "genome only" and "Gag only" constructs. **h**
778 Representative images from before (top) and after (before) photobleaching in HeLa.YFP-
779 A3G cells expressing "genome only" construct. White dashed circles represent regions of
780 targeted photobleaching. **i** Quantification of YFP-A3G fluorescence recovery experiments
781 and zoomed inset of time period over first 80 seconds after photobleaching. All scale bars
782 in fluorescent images = 10μm. Error bars represent standard deviation of the mean.
783

784 **Fig. 4. Viral RNA Genome-A3G interactions are sufficiently strong to redistribute**
785 **A3G to unnatural subcellular locales. a** Schematic of In Cell RNA-protein Interaction
786 Protocol (IC-IP). **b** Schematic of MS2-iRFP constructs used for "targeting" (top) and
787 representative images of MS2-iRFP and YFP-A3G localization in the absence of mRNAs
788 encoding MSL cassette. White arrows point to characteristic subcellular targets of Src-
789 (vesicles) and Lifeact- (filamentous actin) MS2-iRFP. **c** Schematic of IC-IP RNA Bait –
790 Vifxx two-color self-tagging HIV construct. **d** Representative images showing Free MS2-
791 iRFP-NLS, MS2-RFP-NLS, YFP-A3G, and Gag-CFP accumulating at PM-adjacent
792 assembly sites (top). (Middle) Src-MS2-iRFP accumulates at intracellular/perinuclear

vesicles, recruits MS2-RFP-tagged RNA genomes, YFP-A3G, and Gag-CFP. (Bottom) Lifeact-MS2-iRFP induces similar accumulation at actin filaments. Region of interest (ROI) shows YFP-A3G signal in dashed white boxes with arrows highlighting assembly sites (top), vesicles (middle), and linear filaments (bottom). **e** Quantification of re-localization of YFP-A3G phenotypes (*n* = > 90 cells per condition) in the presence of NLS, Src-, and Lifeact-MS2 targeting constructs and **f** percentages of YFP-A3G per cell signal (IntDen) relocalized by Src- and Lifeact-MS2 constructs (*n* > 6). All scale bars in fluorescent images = 10μm, except in A3G ROI insets scale bars = 1μm. Error bars represent standard deviation of the mean.

Fig. 5. Recruitment of YFP-A3G is specific to HIV-1 RNA genome, Gag-independent, and occurs long before the onset of virus particle assembly. a and c Schematics of "genome only" and "Gag only" IC-IP bait constructs, respectively. **b** Representative images showing normal co-distribution of MS2-RFP tagged RNA genomes and YFP-A3G (top) and retargeting of YFP-A3G to intracellular vesicles with RNA genomes by Src-MS2-iRFP (bottom). **d** Representative images showing Src-MS2-RFP accumulating at intracellular vesicles and a complete lack of YFP-A3G at these same sites (white arrow). **e** Time-lapse images of cells expressing "genome only" construct retargeted by Src-MS2-iRFP over a period of 4 hours. T=0 represents the first detection of MS2-RFP genome proxy. Arrow shows accumulation of YFP-A3G at Src-MS2-iRFP+ vesicles as early as 2 hours after the onset of MS2-RFP expression. All scale bars in fluorescent images = 10μm.

Fig. 6. Membrane-targeted APOBEC3G recruits HIV-1 RNA genomes and can inhibit virus particle production. a Schematic of Reciprocal IC-IP using Src-YFP-A3G targeted to intracellular membranes. **b** and **c** Schematic of Vifxx two-color HIV (**b**) and "genome only" (**c**) constructs and representative images showing Src-YFP-A3G (**b**) or Src-CFP-A3G (**c**) recruiting MS2-RFP tagged genomes to intracellular vesicles (white arrows). **d** Schematic of Vifxx Luc HIV infectious single-cycle virus used to infect HeLa.Src-YFP-A3G cells and representative images of FISH/IF detecting *gag-pol* mRNA and Gag p-24, respectively. White arrows highlight sites where Src-YFP-A3G has recruited *bona fide* HIV RNA genomes. **e** Western blot showing dose-dependent inhibition of HIV virus particle assembly and production from HEK293T cells transfected with Vifxx two-color construct, Src-MS2-YFP (lanes 1 and 2), YFP-A3G (lane 3) and Src-YFP-A3G (lanes 4 and 5). Graph shows relative release factor as the ratio of Gag in virus-like particles (VLPs) divided by Gag in cellular lysates quantified from three independent experiments. All scale bars in fluorescent images = 10μm. Error bars represent standard deviation of the mean.

Fig. 7. Cytoplasmic A3G-genome interactions promote consistent per virion delivery of A3G into progeny virions. a Schematics of constructs used in single virion analysis (SVA) studies. **b** Western blot showing cellular expression, YFP-A3G packaging, and Gag assembly and release of constructs depicted in a. **c** Representative images of single fluorescent virion images harvested from HEK293T.YFP-A3G cell line. Scale bar = 500nm. **d** Quantification of SVA for each of the four constructs showing percent of virions with MS2-RFP signal (pink) and YFP-A3G (green). Error bars represent standard

839 deviation of the mean (*n* > 13,000 virions per condition). **e** Relative YFP-A3G signal per
840 virion or virus-like particle derived from Vifxx two-color or COGag conditions. Relative
841 values are normalized to the mean value for Vifxx with means (solid lines) and 25th and
842 75th quartiles (dashed lines) indicated.

SUPPLEMENTARY MATERIAL

Fig. S1. Graphical abstract. Summary of single-cell live imaging approaches used and key findings.

Video 1. Time-lapse imaging of HeLa-.FP-A3G cells infected with Vif+ HIV-1/CFP virus. Multi-channel images of HeLa.YFP-A3G cells were acquired every 60 minutes for 49h after infection. In the highlighted cell, viral gene expression (cyan) is detected ~16hpi with YFP-A3G degradation green0 at 21hpi. This cell rounds up at 28 hpi consistent with Vif-induced G2/M cell cycle arrest.

Video 2. Time-lapse imaging of HeLa.YFP-A3G cells infected with Vifxx HIV-1/CFP virus. Multi-channel images were acquired every 60 minutes for 49h after infection. In the highlighted cell, viral gene expression (cyan) is detected ~19hpi with detection of YFP-A3G (green) at virus particles (arrows) starting at ~25hpi. An example of a transfer event wherein a large cluster of YFP-A3G+ virus particles is released from an infected cell is highlighted (arrows) at 32-36hpi.

Video 3. Time-lapse imaging of HeLa.YFP-TIA1 cells infected with Rhinovirus A16. Multi-channel images were acquired every 30 minutes after addition of RVA16 (MOI~10). The first instances of SG formation (YFP-TIA1 in green) are evident at ~11hpi.

Video 4. Time-lapse imaging of HeLa.YFP-A3G cells expressing the two-color Vif+ Gag-CFP/MS2-RFP HIV-1 reporter virus. Multi-channel images were acquired every 60 minutes for 24h beginning ~4h post-transfection. Left panel shows genome tracked using MS2-RFP (magenta), with nuclear export detected at T=4h just prior to the onset of Gag-CFP (cyan) expression (right panel) and YFP-A3G (green) degradation (center panel).

Video 5. Time-lapse imaging of HeLa.YFP-A3G cells expressing the two-color Vifxx Gag-CFP/MS2-RFP HIV-1 reporter virus. Multi-channel images were acquired every 60 minutes for 24 hours beginning ~4 hours post-transfection. Left panel shows genome tracked using MS2-RFP (magenta), with nuclear export detected at T=6h just prior to the onset of Gag-CFP (cyan) expression (right panel) and co-accumulation of YFP-A3G (green, center panel) with genome (MS2-RFP) and Gag-CFP at the plasma membrane (at putative sites of virus particle assembly).

Video 6. Time-lapse imaging of HeLa.YFP-A3G cells co-expressing "genome only" MS2-RFP HIV-1 reporter virus with the Src-MS2-iRFP targeter (orange). Multi-channel images were acquired every 60 minutes for 15h starting ~4h post-transfection. MS2-RFP tracked genomes (magenta, central panel) are first observed at T=0, with both genomes and YFP-A3G (green, right panel) immediately recruited to perinuclear vesicles, co-localizing with the Src-MS2-iRFP targeter (yellow, left panel). Video demonstrates that genomes have marked effects on YFP-A3G trafficking in the cytosol even at the earliest time points post-genome nuclear export.

FIGURE 1

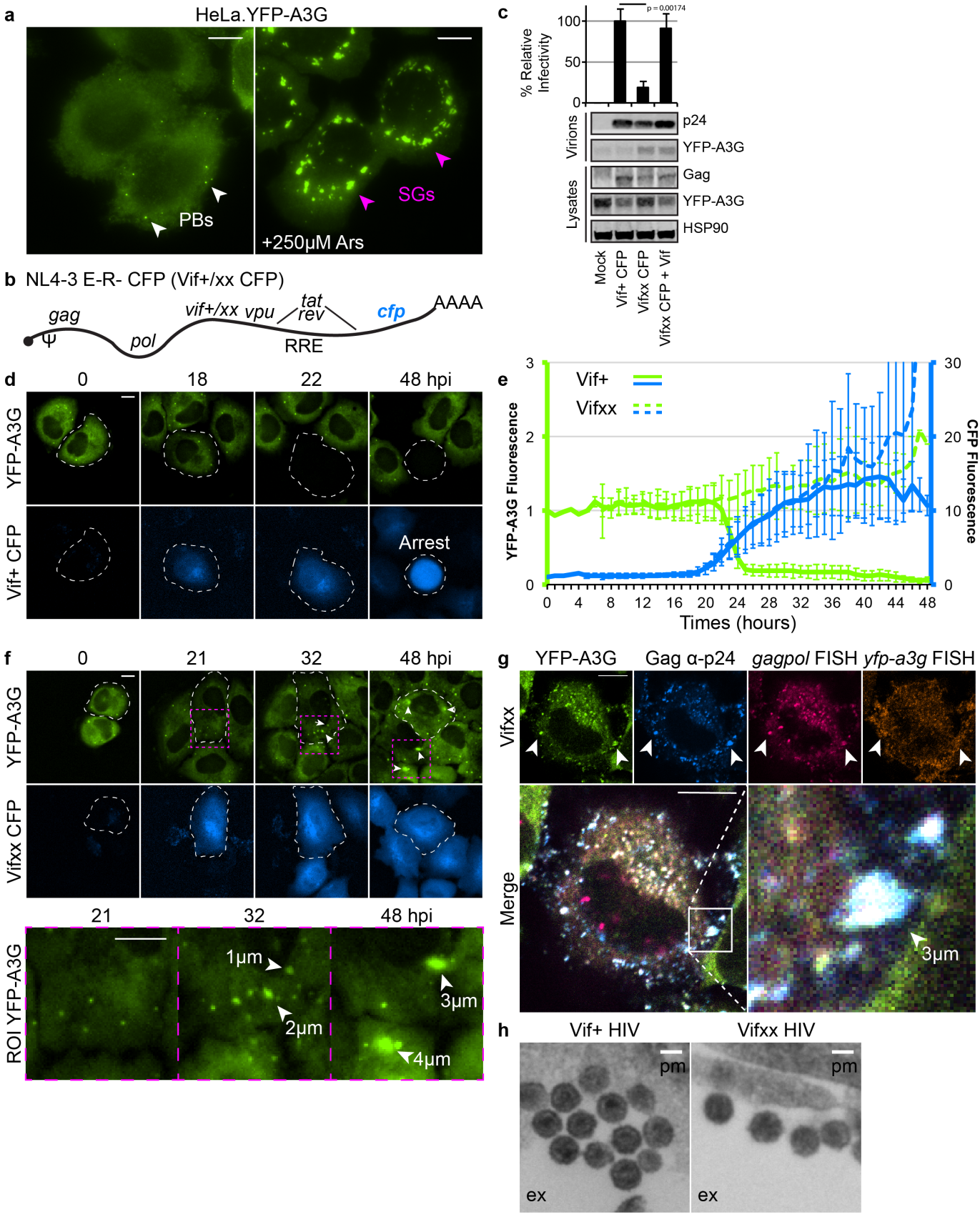

FIGURE 2

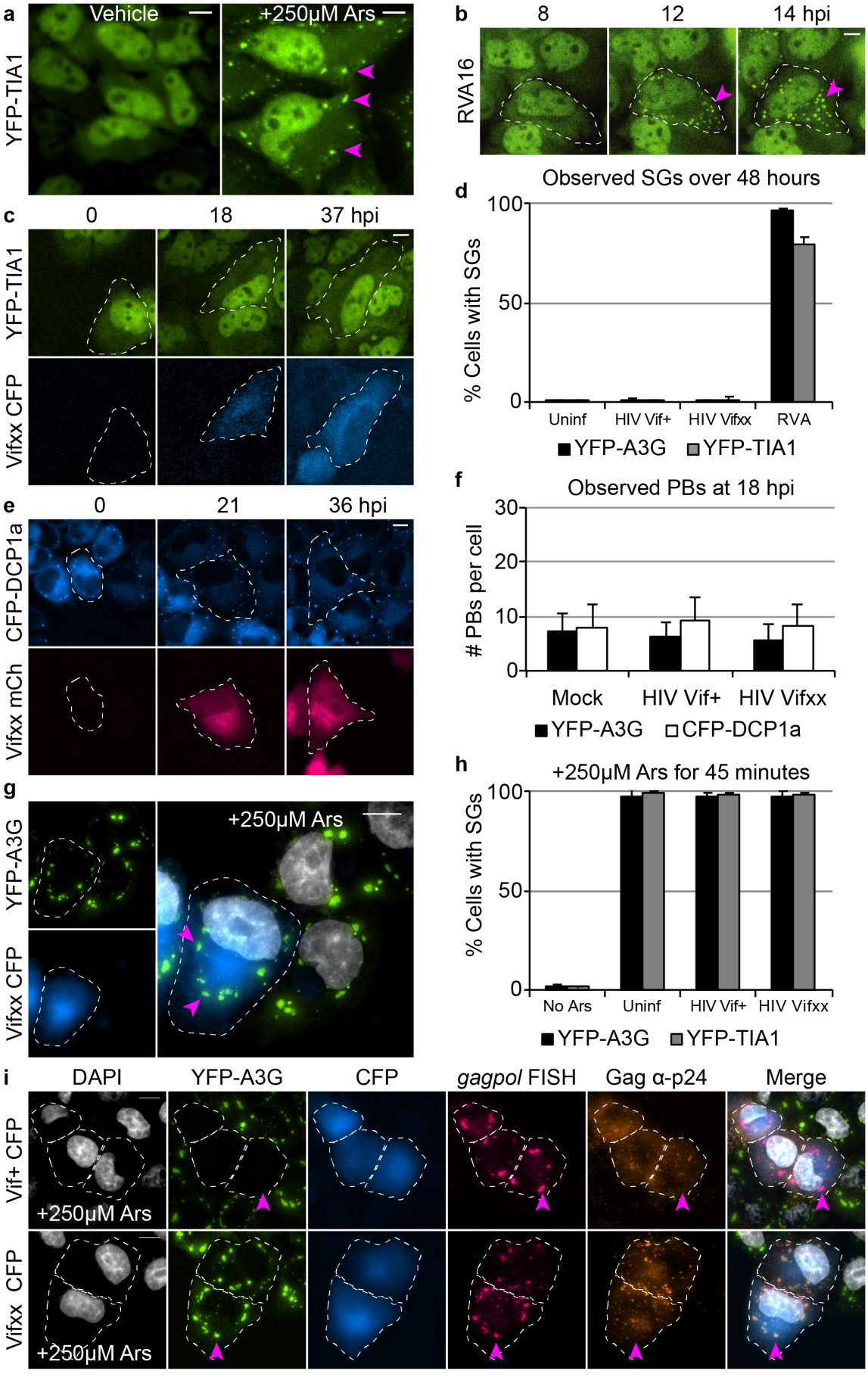

FIGURE 3

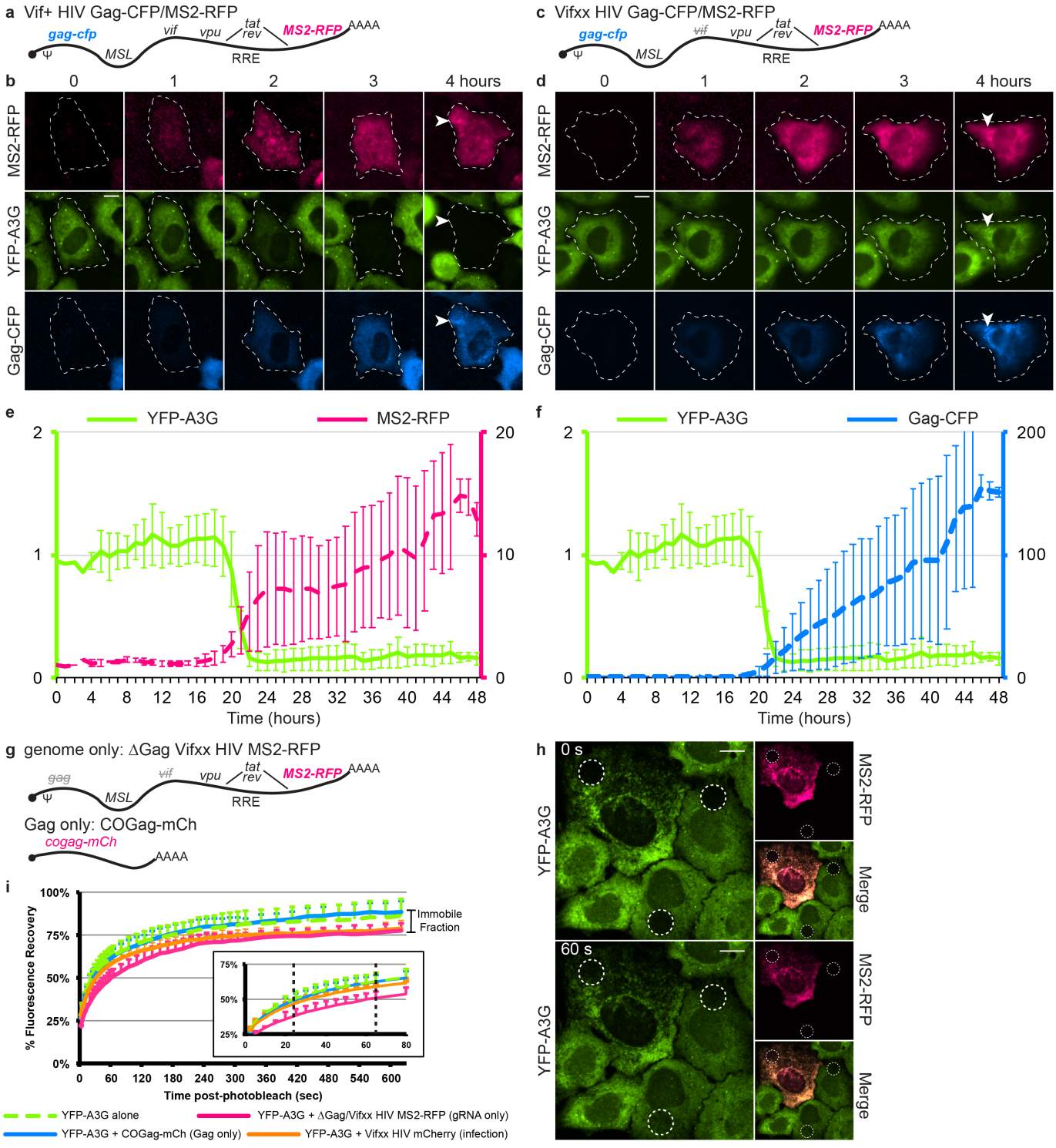

FIGURE 4

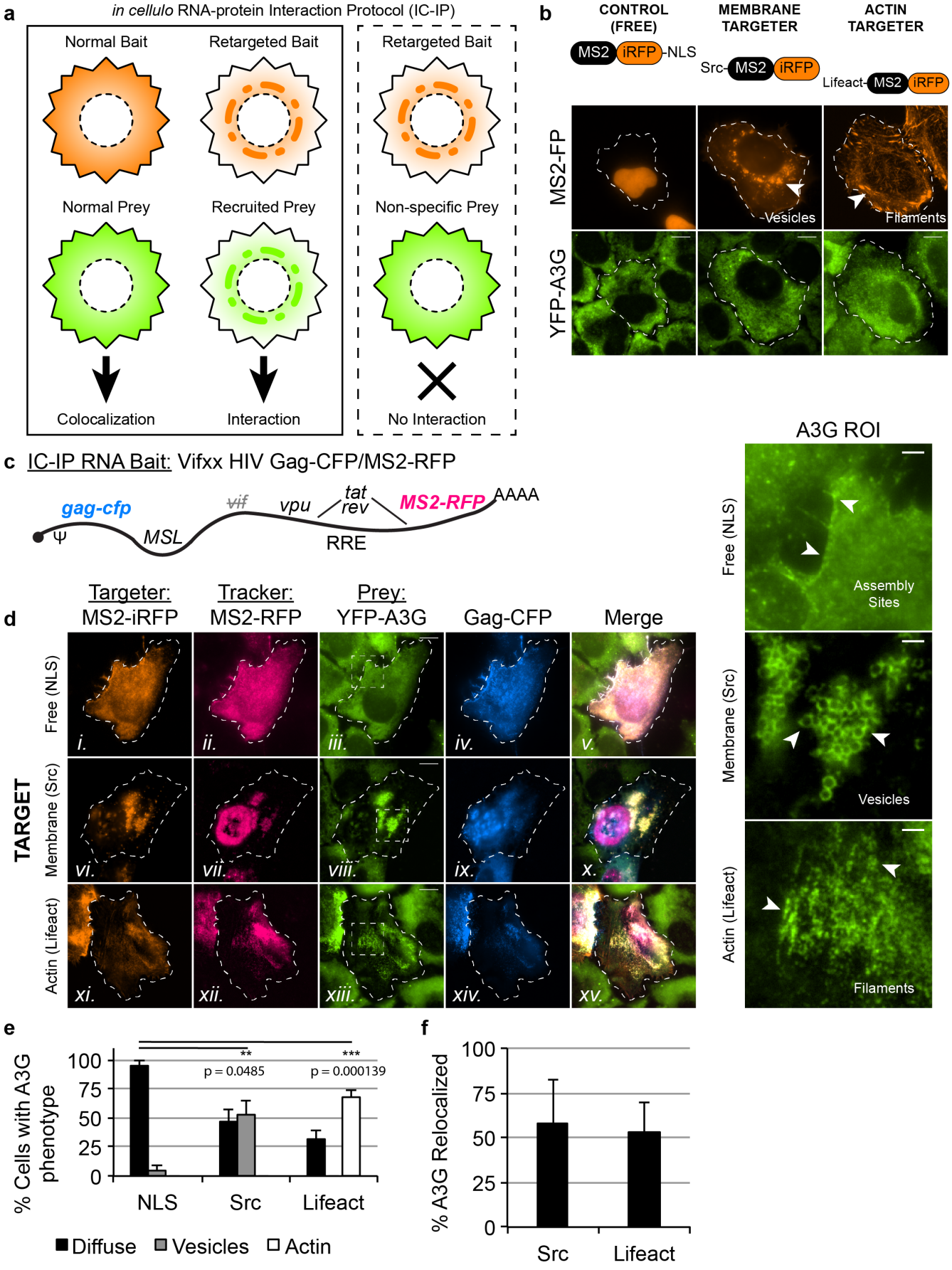

FIGURE 5

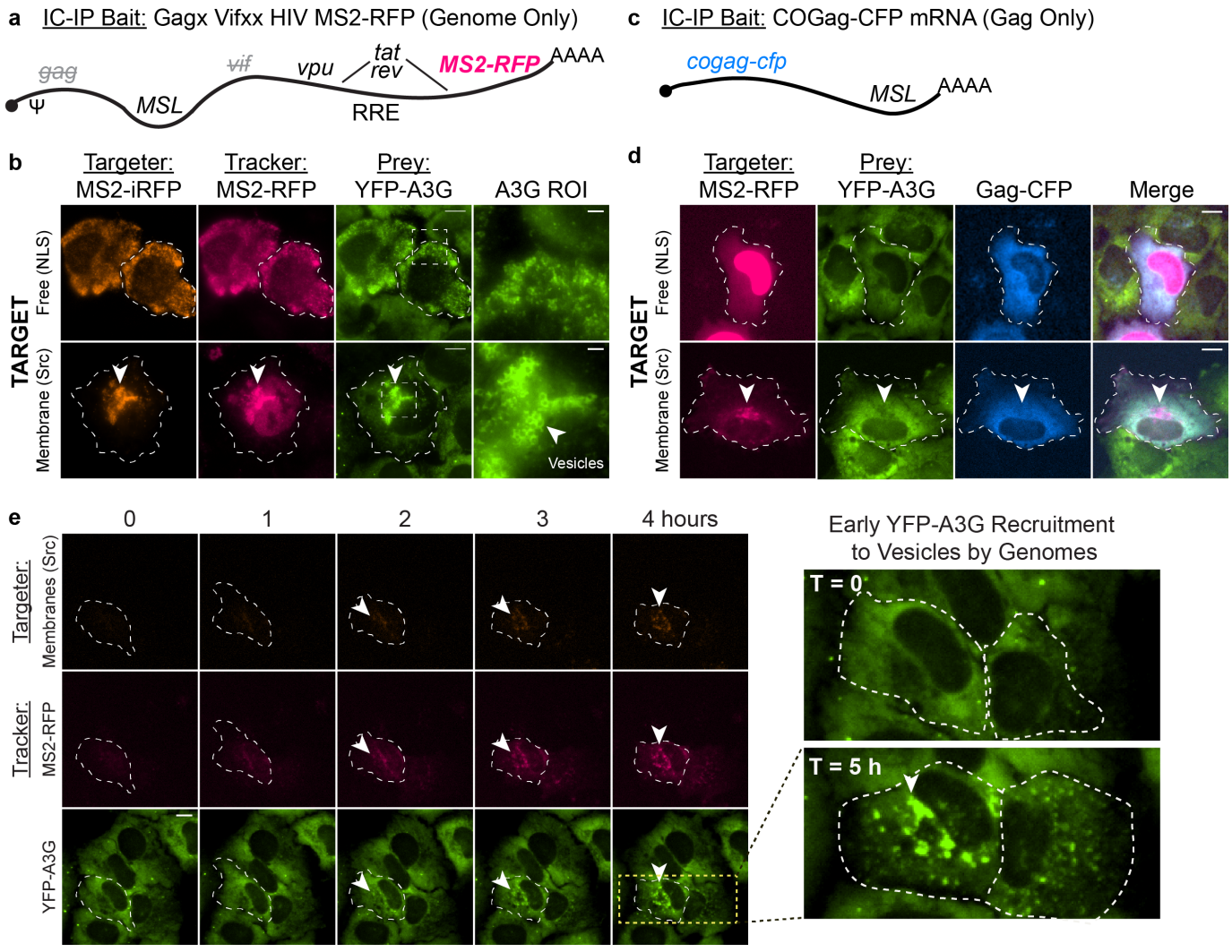

FIGURE 6

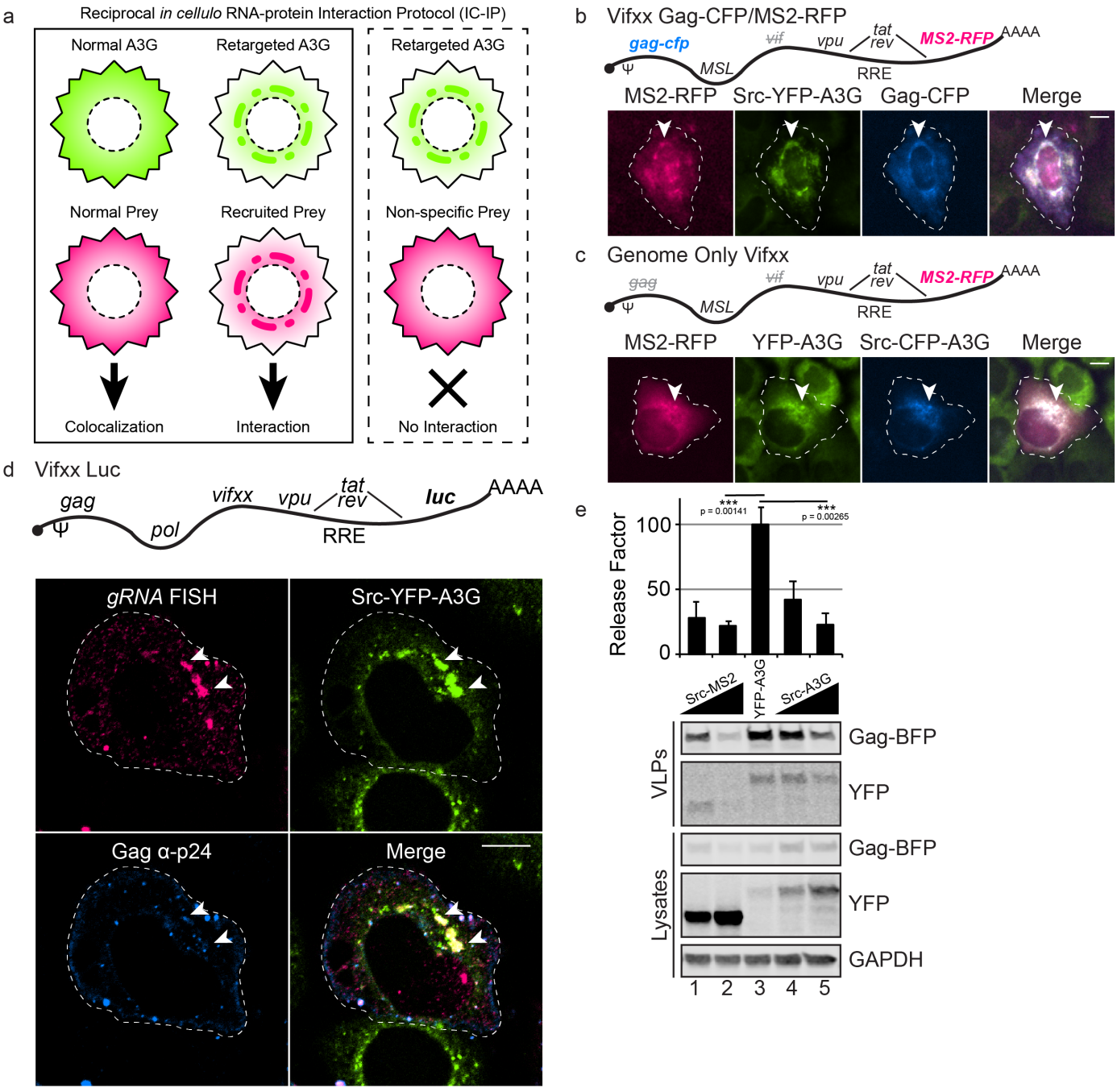

FIGURE 7